Nanoscale Research Letters

RESEARCH

Open Access

Vacuum Evaporation of High-Quality $CsPbBr_3$ Thin Films for Efficient Light-Emitting Diodes

Tianxinyu Bai, Shenwei Wang, Liyuan Bai, Kexin Zhang, Chunyang Chu and Lixin Yi*

Abstract

The all-inorganic lead halide perovskite has become a very promising optoelectronic material due to its excellent optical and electrical properties. Device performances are currently hindered by crystallinity of the films and environmental stability. Here, we adopted dual-source co-evaporation method to prepare $CsPbBr_3$ films. By adjusting and controlling the co-evaporation ratio and substrate temperature, we obtained $CsPbBr_3$ films with large grain sizes and uniform morphology. Films with smooth surfaces and large grains exhibit properties such as efficient photon capture, fast carrier transport, and suppressed ion migration. Therefore, in this paper, by refining the annealing conditions, the effects of annealing temperature and time on the films were studied in detail. The $CsPbBr_3$ films were annealed under suitable annealing temperature and time in ambient air, and films with high quality and crystallinity and average grain size up to ~ 2.5 μm could maintain stability in ambient air for 130 days. The corresponding LEDs show the full width at half maximum (FWHM) of the green EL spectrum is as narrow as 18 nm, and the devices have a low turn-on voltage V_T ~ 3 V and can work continuously for 12 h in ambient air.

Keywords: $CsPbBr_3$, Co-evaporation, Crystallinity, Annealing, Stability

Introduction

Metal halide perovskites of $CsPbX_3$ (X = Br, I, and Cl) have become a research hotspot in recent years due to their many advantages, such as excellent thermal stability [1], extremely narrow emission bandwidth, and tunable band gap [2], and these exceptional properties have also made perovskites suitable for a variety of optoelectronic devices [3, 4], especially light-emitting diodes (LEDs) [5–9] and solar cells [10–12].

The preparation of high-quality inorganic $CsPbBr_3$ perovskite films by a specific method is of great significance for improving the device performance. Researchers usually use solution method to prepare perovskites films. Because of the poor solubility of CsX in the precursor solution, it would be an obstacle for the reproducibility of smooth surface and full coverage $CsPbBr_3$ films [13]; when the solvent is removed by heating, the residual solvent is prone to leak current caused by defects such as pinholes [14], which adversely affects the performance of the device. Therefore, scientists have made a lot of efforts in films optimization, mainly by adding acid or organic ammonium ligands [15–18], interfacial energy modification [19], optimizing precursor solutions [20], and other methods to improve the surface morphology of the films. Cao and co-workers introduced amino-acid additives into the perovskite precursor solutions [21], and the additives can effectively passivate perovskite surface defects and reduce non-radiative recombination, so the prepared perovskite films with the sharp and strong diffraction peaks indicate that the crystallization quality has been improved. Rogach and co-workers used cesium trifluoroacetate (CsTFA) as the cesium source, instead of the commonly used cesium bromide (CsBr) [22]. The CsTFA-based precursor produced smooth, fully covered

*Correspondence: lxyi@bjtu.edu.cn

Institute of Optoelectronic Technology, Beijing Jiaotong University, Beijing 100044, China

perovskite films with improved photoluminescence quantum yield.

The vacuum evaporation method can easily deposit multilayer films with good flatness and morphology [23], however, which is less reported. Here, we report the use of dual-source vacuum co-evaporation to prepare $CsPbBr_3$ films. During the lengthy deposition process (usually 2–3 h), it is difficult to maintain a correct ratio of evaporation rates of source materials throughout the process because the experimental conditions fluctuate [24], so adjusting and controlling the ratio of evaporation rates of source materials is key of co-evaporation. By adjusting the co-evaporation ratio and substrate temperature, highly phase-pure $CsPbBr_3$ is successfully fabricated and the surface morphology of the films was well regulated. Moreover, perovskite films with large grain sizes have fewer internal grain boundaries. Therefore, large grain sizes, uniform density, high crystallinity are properties of high-quality perovskite films. Devices of perovskite thin films with these properties usually have higher efficiency and stability, so how to prepare the thin films with large grain sizes has become one of the hot spots of scientific researchers. Here, $CsPbBr_3$ films were annealed under suitable annealing conditions in ambient air. It should be pointed out that in most of the other studies, the annealing process of vacuum-deposited inorganic $CsPbBr_3$ films was carried out under nitrogen atmosphere [10, 13, 25, 26]. In addition, the $CsPbBr_3$ films achieved high luminescent intensity and smooth morphology and the average grain sizes over 2.5 μm. What's more, the films had superior stability, which maintained optical properties in ambient air for more than four months. The corresponding LEDs showed the full width at half maximum (FWHM) of the green EL spectrum was as narrow as 18 nm, and the devices had a low turn-on voltage $V_T \sim 3$ V and can work continuously for 12 h in ambient air, a maximum luminance (L_{max}) of 252 cd m^{-2}. It provides a good foundation for its application in later device.

Experimental

The substrates were cleaned by deionized water, detergent, acetone, and absolute ethanol and then dried by flowing nitrogen gas. Choose CsBr (99.9%) and $PbBr_2$ (99.9%) powders as the deposition materials; after water removal treatment, they were placed in two thermal evaporation crucibles. The vacuum degree of the evaporation chamber is reduced to 3×10^{-3} pa, and the thickness of the films and the evaporation rate of CsBr and $PbBr_2$ can be monitored by a quartz crystal monitor. To further improve the crystalline quality of the films, the original films were annealed in ambient air (RTP-500) in the range of 400–460 ℃. The PeLEDs have a device structure of Ag (100 nm)/N-type Si/NiO (40 nm)/$CsPbBr_3$ (100 nm)/ITO (100 nm). Firstly, $CsPbBr_3$ films were deposited on N-type Si (100) substrates by thermal co-evaporation (SD400M). Secondly, NiO films as the hole transport layer were deposited on the $CsPbBr_3$ films by magnetron sputtering technique (XSYZKFQ-1200). The sputtering power was 60 W, the gas flow rates of Ar and O_2 were 45 and 10 sccm, volume ratio was 3 mTorr chamber pressure during sputtering, and the sputtering rate was 0.1 Å/s. ITO and Ag electrodes also use magnetron sputtering technique. ITO electrode was deposited on the surface of the films, and the sputtering power was 100 W, the Ar airflow rate was 40 sccm, and the sputtering rate was 0.6 Å/s. Ag electrode was deposited on the backside of the N-type Si substrate, the sputtering power was 150 W, the Ar gas flow was 40 sccm, and the sputtering rate was 9 Å/s.

Absorption spectra of the $CsPbBr_3$ films were recorded using an UV–VIS–NIR scanning spectrophotometer (UV-3101PC). The photoluminescence (PL) spectra were measured by 325 nm He–Cd laser and a fluorescence spectrophotometer (FLS920) as the light source and detector [27]. Before every measurement, the equipment is calibrated to ensure high accuracy and reliability. The crystallinity and phases of films were examined by the X-ray diffraction (XRD, Bruker D8 Advance) pattern. The surface morphologies of thin films were observed by scanning electron microscope (SEM, Hitachi, SU8020).

Results and Discussion

Control of Evaporation Rate Ratio

The evaporation rate is a key factor that affects the stoichiometric ratio of the source material and the performance of the device. The competition between how fast atoms on the surface migrate and how quickly the next atoms arrive on the surface and form an immobile cluster with the existing atoms (i.e., deposition rate) is the primary determining factor of the films morphology [28]. Since the co-evaporation method cannot monitor the molar ratio incident on the substrate surface, in order to obtain $CsPbBr_3$ films with the correct element ratio, the evaporation rate ratio of the two precursors need to be better adjusted and controlled [13].

First, we studied the effect of evaporation ratio on the crystal structure of perovskite films. Figure 1 shows the XRD patterns of $CsPbBr_3$ films with different evaporation rate ratios (1.14:1–4:1). When the evaporation rate ratio of $PbBr_2$ to CsBr is 1.14:1, an additional peak at 29.8°appears, which assigns CsBr phase (PDF#05–0588). It is also found in energy-dispersive spectrometer (EDS) data. As shown in Table 1, when the $PbBr_2$ and CsBr evaporation ratio reaches 1.14:1, the atomic percentages of Cs, Pb, and Br in the $CsPbBr_3$ films are 31%, 11%, and 58%, respectively. The Pb element percentage is

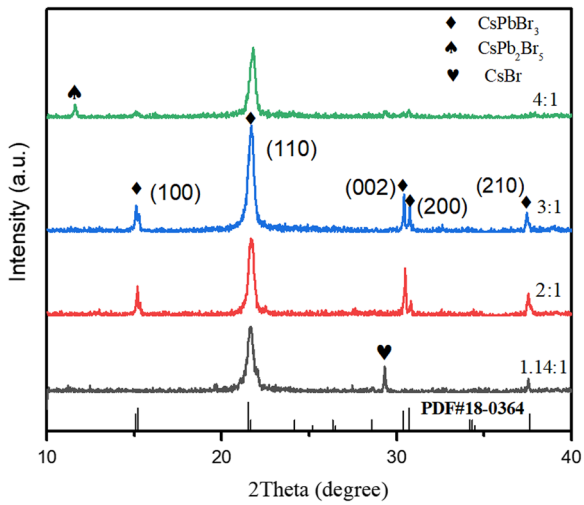

Fig. 1 XRD patterns of $CsPbBr_3$ films with different evaporation rate ratios

Table 1 Analysis of the element ratio of $CsPbBr_3$ thin films prepared under different evaporation rate ratios

Element	Evaporation ratio ($PbBr_2$:CsBr)			
	Atomic percentage			
	1.14:1	2:1	3:1	4:1
Br	58.40	62.07	62.43	64.39
Cs	30.80	20.66	18.46	16.22
Pb	10.78	17.27	19.12	19.39
Total	100.00	100.00	100.00	100.00

significantly lower than the theoretical value (20%, 20%, 60%), causing by the $PbBr_2$ powders loss during deposition process [23].

In order to increase the Pb ratio in $CsPbBr_3$ films, we adjusted the evaporation rate ratio of $PbBr_2$ to CsBr. When the evaporation rate ratio is 3:1, the peaks at $2\theta = 15.1°$, 15.3°, 21.5°, 30.4°, 30.7°, and 34.2° should be ascribed to the diffraction of (001), (110), (110), (002), (200), and (210) crystal planes (PDF#18–0364), indicating the formation of the cubic $CsPbBr_3$ phase, (110); diffraction peak intensity is stronger for the other ratios, showing that the deposited $CsPbBr_3$ films have the best crystallinity. Moreover, the atomic percentages of Cs, Pb, and Br in the $CsPbBr_3$ films are 18%, 19%, and 62%, respectively. The corresponding ratio of Cs, Pb, and Br is 1:1.1:3.4, which is the nearest to 1:1:3 of $CsPbBr_3$ among all the evaporation rate ratios. However, when the evaporation rate ratios continue to increase, $CsPb_2Br_5$ phase appears, and the element proportion mismatches, as shown in Table 1. As a result, the suitable evaporation rate ratio for $CsPbBr_3$ films is 3:1 of $PbBr_2$ to CsBr.

Figure 2a shows the optical properties of $CsPbBr_3$ films with co-evaporation rate ratio of 3:1, containing the PL and absorption spectrum. The bright green PL is obtained. The luminescence peak position of the films is 517 nm, with full width at half maximum (FWHM) of 18 nm, and an intrinsic light absorption peak appears at the luminescence peak position.

The optical band gap E_g of the films can be calculated by transmission spectrum. According to the optical coefficient equation [29, 30]:

$$(h\nu\alpha)^{1/n} = A(h\nu - E_g)$$

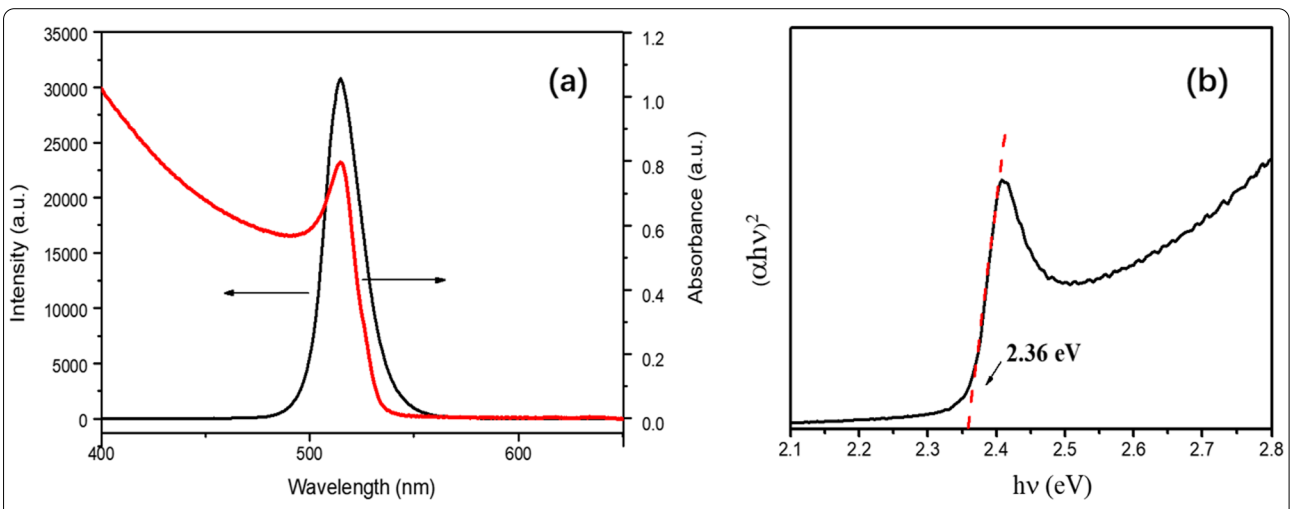

Fig. 2 **a** The PL and absorption spectra of $CsPbBr_3$ thin films **b** Plot of $(\alpha h\nu)^2$ versus hν of $CsPbBr_3$ thin films

where $h\nu$ is the photon energy, α is the absorption coefficient, E_g is the optical band gap, A is the proportional constant, and the value of exponent n depends on characteristic of materials, n = 1/2 and 2 for direct and indirect band gaps, respectively. $CsPbBr_3$ materials are used as a direct-gap semiconductor, and n should be equal to 1/2. Taking the linear region of $h\nu$-$(\alpha h\nu)^2$ curve and drawing the reverse tangent [31], as shown in Fig. 2b, the optical band gap of the films is calculated to be 2.36 eV, which is basically consistent with the other relevant report [32, 33].

Study on the Substrate Temperature of the $CsPbBr_3$ Thin Films

As for vacuum co-evaporation, the substrate temperature not only affects crystal growth dynamics, but also influences the sticking coefficient, which further changes the migration rate of atoms on the films surface [34]. Moreover, the crystal grain size and morphology of the films are controlled by adjusting the substrate temperature, so as to obtain a smoother surface morphology. We studied the effect of substrate temperature (room temperature (RT) – 175 °C) on the crystallinity of the $CsPbBr_3$ films. XRD patterns of $CsPbBr_3$ films at different substrate temperatures are shown in Fig. 3a; when the substrate temperature is 150℃, (110) crystal plane exhibits the strongest diffraction intensity and extremely narrow diffraction half-width, indicating that the $CsPbBr_3$ films deposited at this temperature have the best crystallinity. Figure 3b depicts optical properties of thin films at different substrate temperatures, including PL spectra. Under 325 nm excitation, the thin films all show an obvious luminescence peak near 517 nm, and the light intensity is the strongest when the substrate temperature is 150℃, demonstrating that this $CsPbBr_3$ film shows the highest photogenerated carrier efficiency, which is also consistent with the results obtained from XRD patterns. Therefore, substrate temperature of 150 ℃ is the optimal growth condition of thin films.

Surface morphology of the $CsPbBr_3$ thin films at different substrate temperature is exhibited in Fig. 4. It can be seen that increase in the substrate temperature can indeed improve crystallinity and grain sizes of the films. The average grain sizes become much larger, and the films become more compact. These are mainly because the atoms and molecules get higher energy, so they are more likely to migrate and rearrange on the substrate surface and tend to move to the thermodynamic equilibrium position, so the films become more compact. When the substrate temperature reaches 175℃, although the adsorbed atoms have high kinetic energy, the evaporation of atoms on the substrate surface is intensified due to the high temperature, and part of $CsPbBr_3$ grains is decomposed, so the uneven grain size leads to the decrease in the crystallinity of the films.

Effect of the Rapid Annealing on the $CsPbBr_3$ Thin Films

Annealing Temperature

In order to further improve the grain size and crystallinity of $CsPbBr_3$ films, the as-deposited $CsPbBr_3$ films (deposited at optimal evaporation rate ratio of 3:1 and

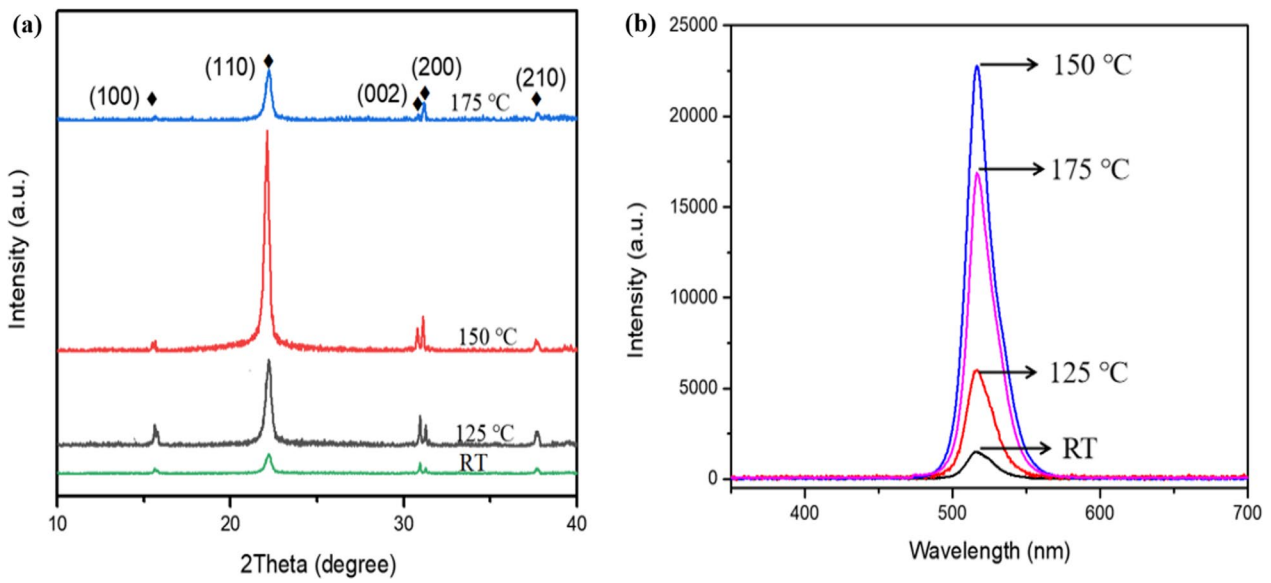

Fig. 3 **a** XRD patterns, **b** PL spectra of $CsPbBr_3$ films at different substrate temperatures

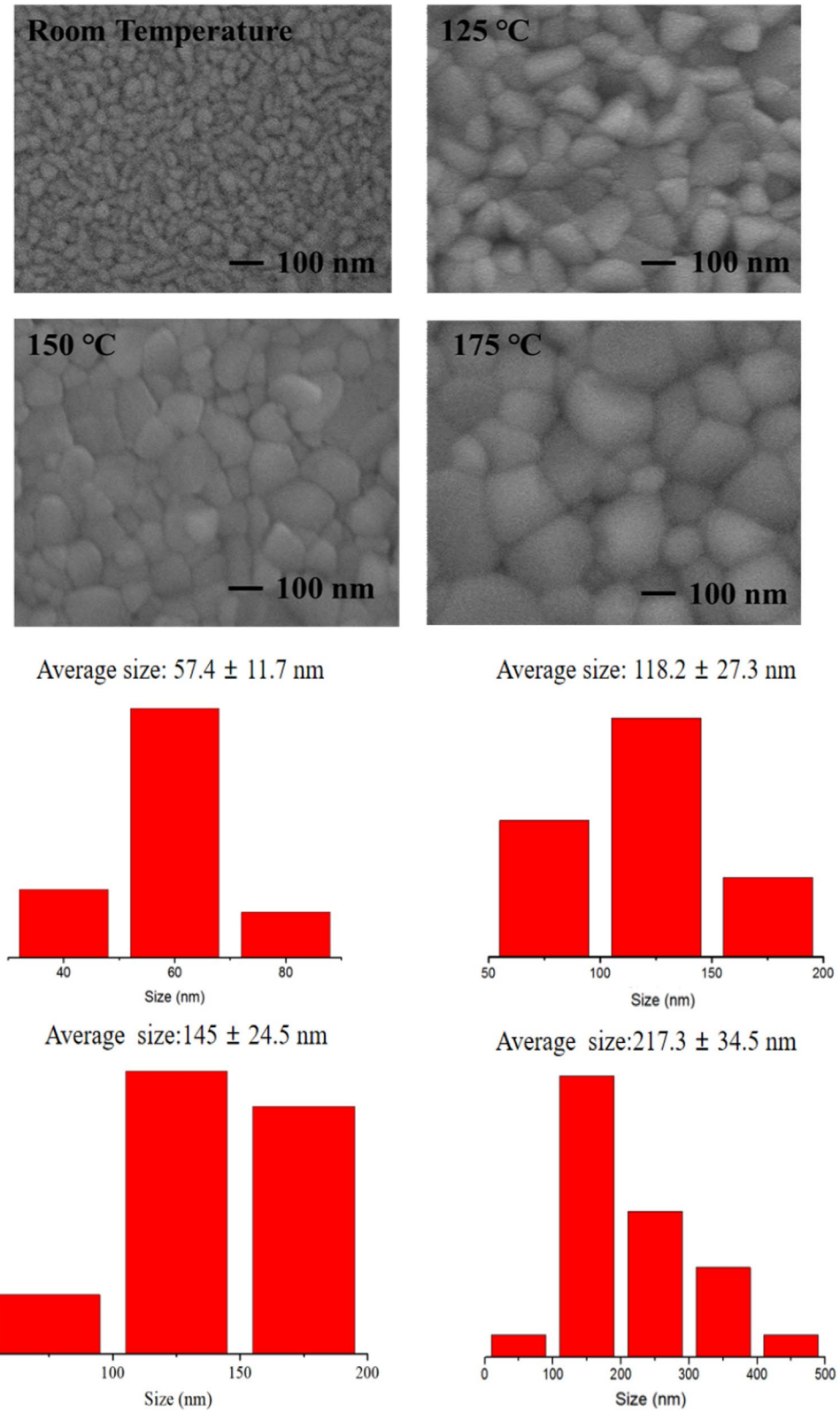

Fig. 4 SEM spectra and particle size distribution of $CsPbBr_3$ films at different substrate temperatures

substrate temperature of 150 ℃) were submitted to a post-annealing process. To investigate how annealing temperature affects the crystallization of $CsPbBr_3$ perovskite, we adjusted the temperature value from 400 to 480 ℃.

As shown in Fig. 5. The characteristic peaks of $CsPbBr_3$ at $2\theta = 15.2°$, 21.6°, 30.37°, and 30.7° correspond to (100), (110), (002), and (200) crystal planes (PDF#18–0364), respectively, indicating the formation of cubic crystal phase. When the annealing temperature is 460℃, the intensity of diffraction peak is the strongest, indicating that the $CsPbBr_3$ films deposited at this temperature have the best crystallinity. During annealing process, the preferential crystal orientation changed from (110) to (100) and (200). Annealing alters the crystallization kinetics of perovskite, driving $CsPbBr_3$ films recrystallize, transferring to a more stable structure. In addition, with the increase in annealing temperature, the intensity of XRD diffraction peaks is increased, indicating improved crystallinity of the $CsPbBr_3$ films.

During the deposition process, various defects and vacancies in the films will increase. Internal stress generally exists in the thin films, which affects the device performance. At present, it is generally accepted that the internal stress can be divided into thermal stress and intrinsic stress. To put it in detail, rapid annealing mainly influences thermal stress of films. When extra heat is applied to the perovskite, dislocations can compound in the films, crystallinity improved, and the thermal stress in the films reduces. Under high-temperature annealing, the cooling rate is too fast, and the thermal stress is difficult to release. Therefore, annealing to reduce or eliminate the thermal stress in the thin films can improve the crystallinity of the $CsPbBr_3$ films and further achieve the higher-performance devices [35–38].

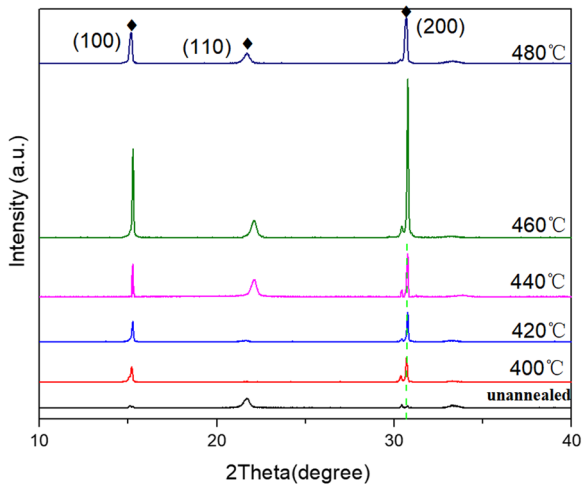

Fig. 5 XRD patterns of $CsPbBr_3$ thin films annealed at different temperatures

The impact of the annealing temperature on the films morphology was examined with scanning electron microscope (SEM), as shown in Fig. 6. The $CsPbBr_3$ films are composed of dense crystal grains with a complete surface coverage. The as-deposited $CsPbBr_3$ films have small grain sizes, with an average grain sizes of 100 nm. When the annealing temperature is 420 ℃, most of the $CsPbBr_3$ grains grow up to 400–600 nm, and the films surface becomes flatter. By further increasing the annealing temperature, we find the grain sizes of $CsPbBr_3$ continue to grow. When the annealing temperature is 440℃, a large number of $CsPbBr_3$ crystals with grain sizes can reach 1 μm, and the pinholes nearly disappear. The increase in grain sizes and the elimination of pinholes are mainly attributed to the external heat energy. The vacancies, interstitial atoms, and dislocations that were originally "frozen" migrate to the surface or grain boundaries and disappear. A large number of non-equilibrium defects disappear so that the thermal stress is released. In addition, when the annealing temperature is high enough, the grains in the films undergone a various recrystallization, which increases the grains and further reduces the grain boundaries [37, 38]. When the annealing temperature is 460 ℃, the $CsPbBr_3$ grains are very large (1.5 μm-3 μm). Annealing is beneficial for $CsPbBr_3$ films reconstruction and recrystallization. As large grains annex small grains, average grain sizes increase. As a result, the films become flatter and crystallinity improved [39].

The optical and photoelectric properties of the $CsPbBr_3$ films are studied by photoluminescence (PL) spectra, as shown in Fig. 7a. The PL peak position is determined by the band gap width of $CsPbBr_3$ films. Therefore, the PL peak of the films appears near 520 nm in the visible region, maintaining the characteristics of direct band gap transition. As the annealing temperature increases, the PL intensity strengthens constantly, but once annealing temperature exceeds 460 ℃, the intensity weakens. The enhanced PL intensity can be attributed to the improved crystallinity of the films. By using bi-exponential decay function, the curves are fitted to determine the fast decay times (τ_1) and slow (τ_2) components [40, 41]. Using a bi-exponential decay function $F(t) = A_1\exp(-t/\tau_1) + A_2\exp(-t/\tau_2) + A_0$ [42]. The average carrier lifetimes of unannealed, 400, 420, 440, 460, and 480 ℃ annealed $CsPbBr_3$ films are calculated to be 0.79, 0.90, 0.93, 2.52, 6.3, and 4.0 ns, respectively. The $CsPbBr_3$ films annealed at 460 ℃ have the longest carrier lifetime, reflecting the best photoelectric

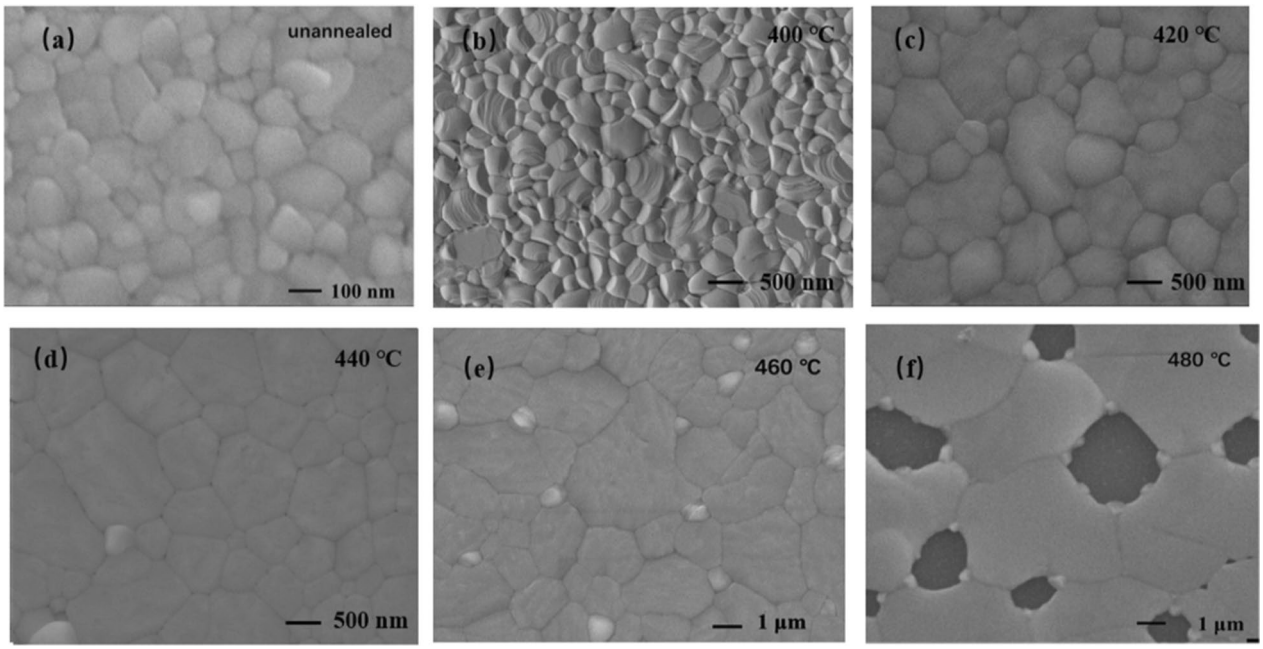

Fig. 6 SEM images of $CsPbBr_3$ films annealed at different temperatures **a** unannealed, **b** 400℃, **c** 420℃, **d** 440℃, **e** 460℃, **f** 480℃

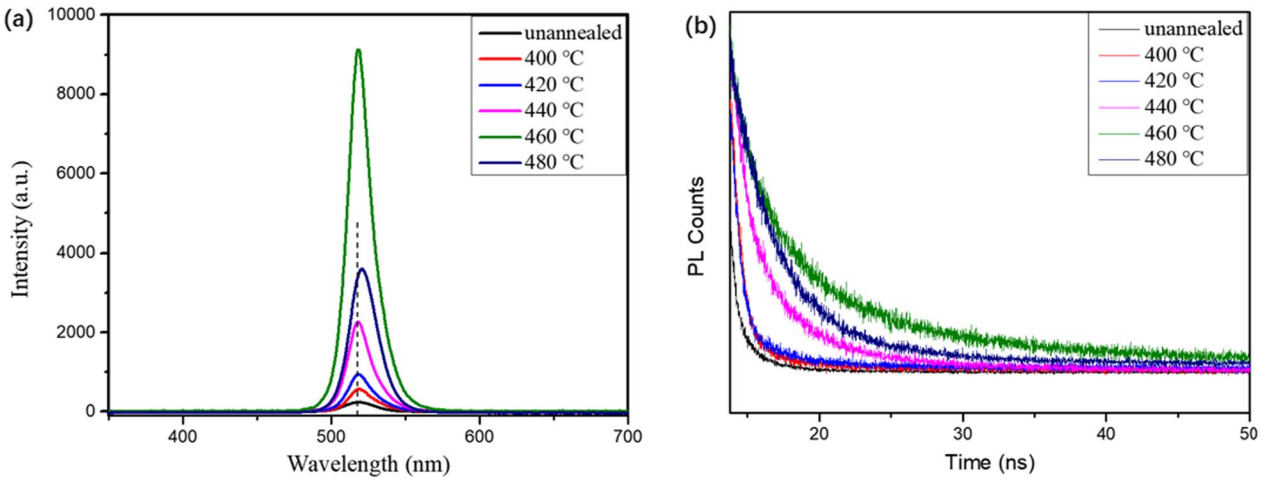

Fig. 7 **a** PL spectrum, **b** time-resolved PL decay curves of $CsPbBr_3$ thin films annealed at different temperatures

quality, and this also coincides with the analysis of SEM and XRD patterns.

Annealing Time

As previously reported, the effect of the annealing conditions on $CsPbBr_3$ films was investigated, including annealing temperature. Figure 8a shows the PL spectra of $CsPbBr_3$ thin films annealed at 460 ℃ for various times from 40 to 100 s in ambient air. Appropriate annealing time is beneficial to improve the grain sizes and photoelectric quality of thin films. As the annealing time increases from 40 to 60 s, the luminescence intensity increases continuously and then decreases. XRD patterns as shown in Fig. 8b and the diffraction intensity of (100) and (200) phases both enhance, and once the annealing time above 60 s and the intensity both recede, the results are consistent with PL intensity.

To further explore the morphology of the films, Fig. 9 shows the SEM images under different annealing times, and the average grain sizes range from ~ 2 to ~ 3.4 μm.

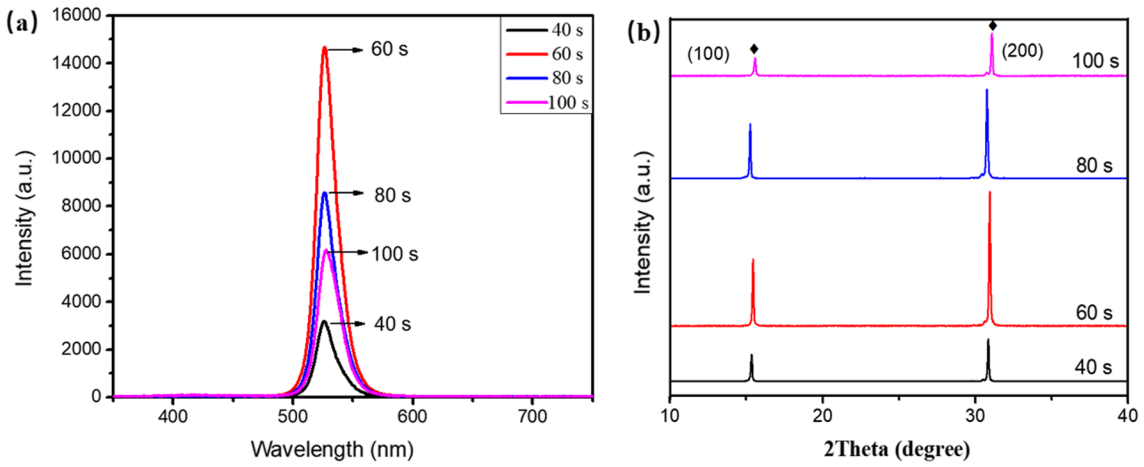

Fig. 8 **a** The PL spectra (λex = 325 nm), **b** XRD patterns of $CsPbBr_3$ films annealed at 460 ℃ for different times

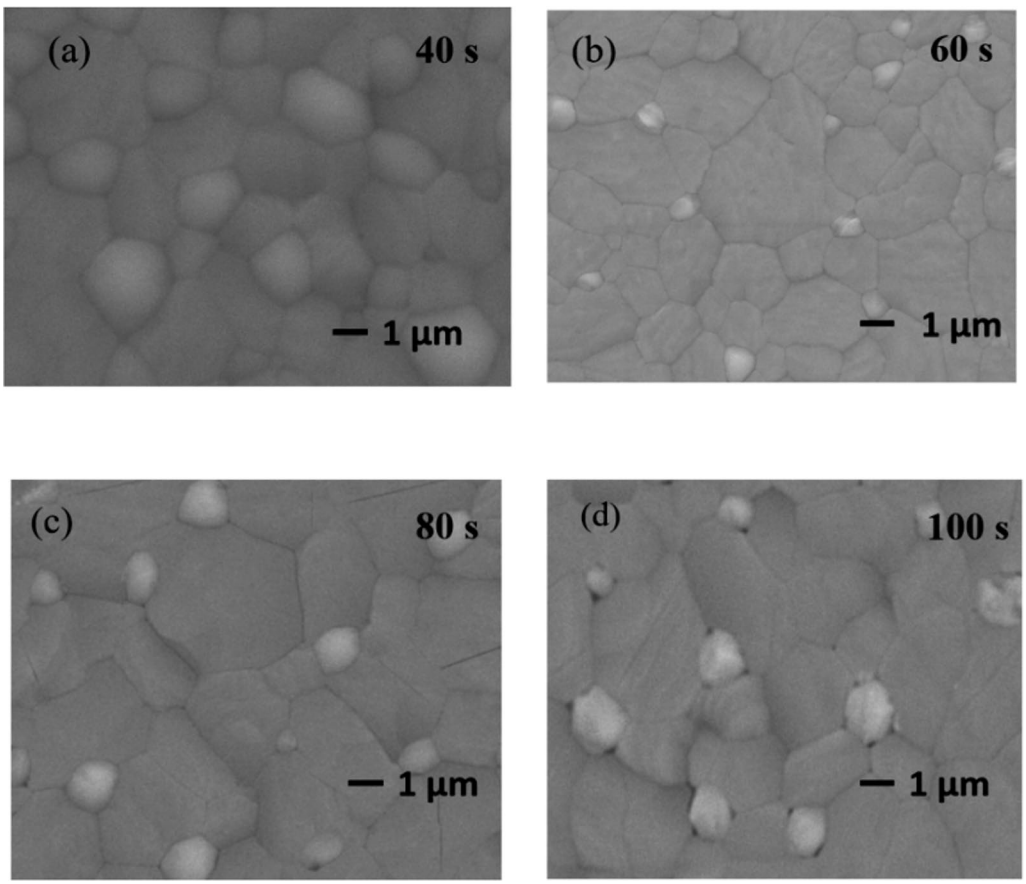

Fig. 9 SEM images of $CsPbBr_3$ films annealed at 460 ℃ for different times

When the annealing time is 60 s, the average grain sizes can reach 2.5 μm. Proper annealing time is helpful to improve the crystallinity of the films. But too long annealing time leads to the grains decomposition, and the element ratio does not meet the requirement of 1:1:3, which reduces PL intensity. So the best annealing

condition is at 460 ℃ for 60 s, which can achieve the strongest PL intensity and the best crystallinity with large grains. These are also consistent with the results obtained by PL spectra and XRD patterns.

Research on the Stability of $CsPbBr_3$ Thin Films

In order to verify the stability of all inorganic halogen perovskite and further optimize the films quality, the annealed samples were placed at room temperature in air atmosphere, the PL intensity was measured about 130 days, as shown in Fig. 10, it can be seen that the PL intensity did not decay so much, and the decay rate was about 13% in the first 75 days. Tiny variation of peak position was assigned to CCD's instrumental error. The effect of long-term storage on peak position was not obvious, and the peak position was still at 517 nm. The PL intensity and peak position of the films remained stable. Therefore, the preparation of $CsPbBr_3$ films by thermal evaporation method and annealing has good stability, which have great potential in improving device performance.

Study on the PeLEDs

Based on the best crystallinity and morphology, PeLEDs were fabricated. The devices architecture is shown in Fig. 11, and perovskite $CsPbBr_3$ layer is the emitting layer of carrier radiation recombination. The working mechanism of the device can be discussed according to the most basic physical progresses of light-emitting diodes [4, 43, 44]. Driven by forward voltage, green electroluminescence of the device is observed under dark conditions, the PeLEDs exhibit good rectification characteristics, the reverse current is small, and the turn-on voltage of the device is ~ 3 V. Figure 12a presents the EL spectrum

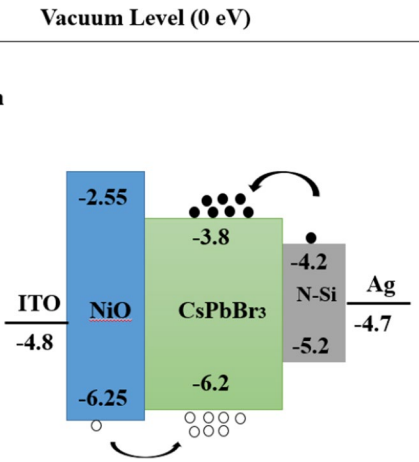

Fig. 11 The working mechanism of the PeLEDs based on the energy band diagram

of the devices, and inset figure is the photograph of our PeLEDs at an injection voltage of 12 V. The spectra show an emission peak at 520 nm with the FWHM of 18 nm, which indicates our PeLEDs have an excellent color purity. Additionally, the devices with annealed $CsPbBr_3$ films show higher EL intensity compared to the unannealed films, which indicates that the surface morphology and crystallinity of the films are helpful to improve the performance of the devices. After annealing, the devices performed best with a maximum luminance (L_{max}) of 252 cd m^{-2}. The results in both L_{max} and EL intensity thus emphasize the importance of films morphology and coverage on device performance. Moreover, the PeLEDs can work continuously for 12 h, and the emission attenuation is ~ 30% in ambient air, with relatively superior stability.

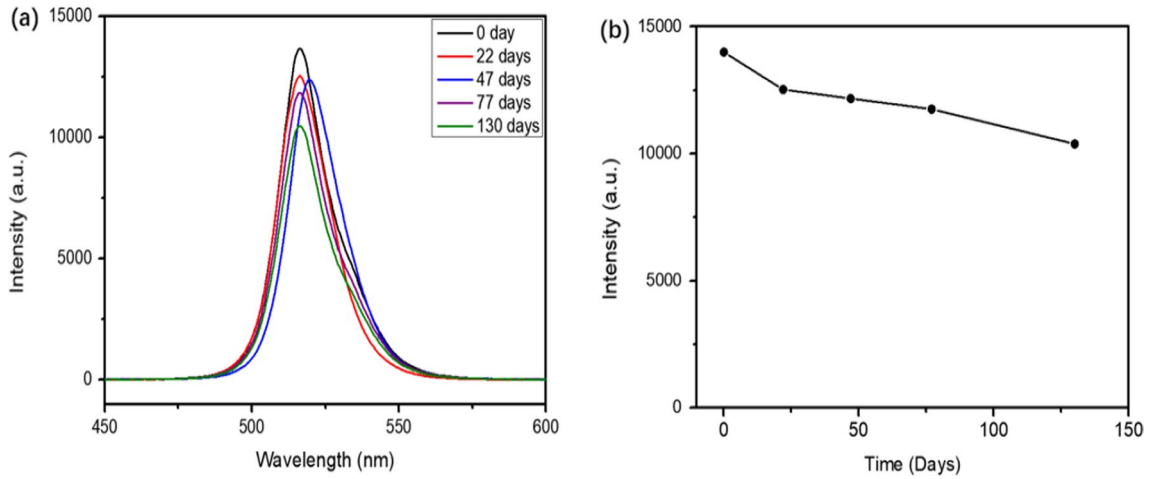

Fig. 10 **a** Peak position of the PL spectrum with different storage times in ambient air (λex = 325 nm). **b** The PL intensity trend

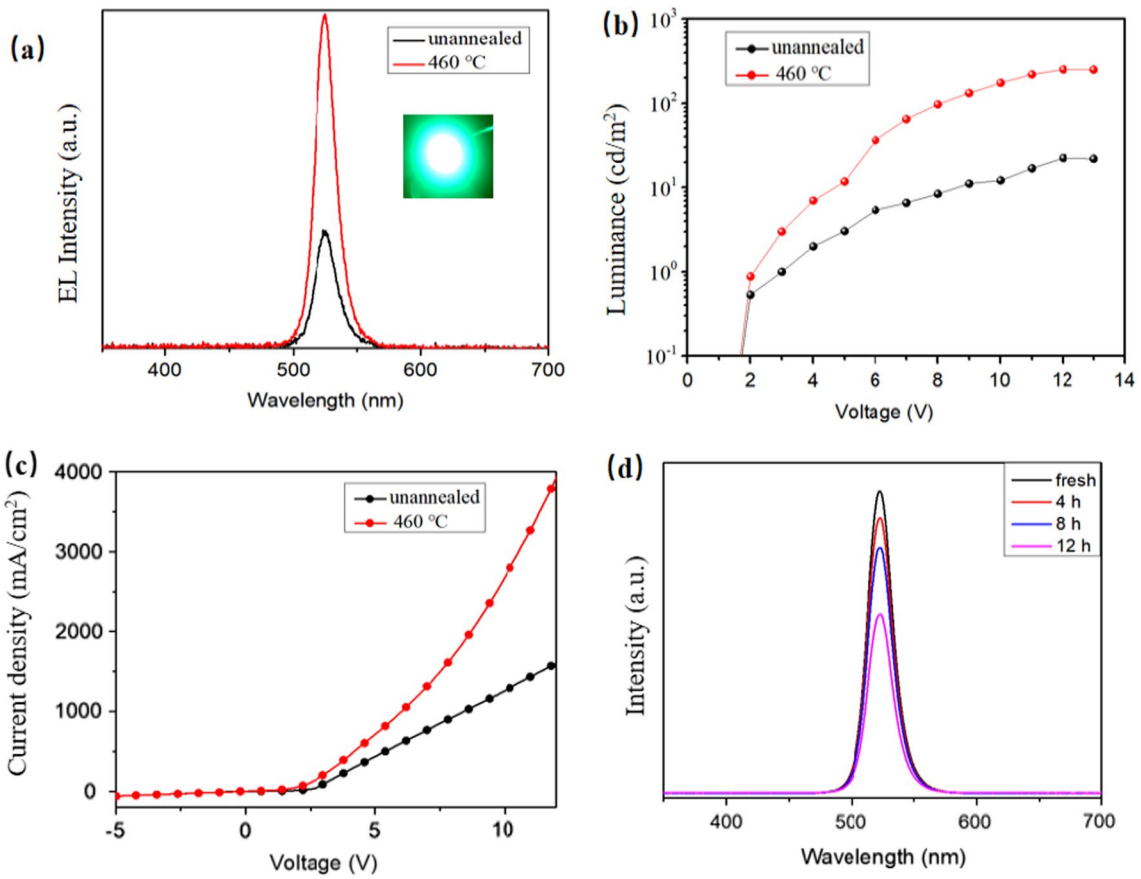

Fig. 12 **a** EL spectra, **b** luminance against voltage (*L*–*V*) curves, **c** current density against voltage (*J*–*V*) curves of PeLEDs, and **d** EL spectra acquired at different operating cycles under the same bias and measurement conditions

Conclusion

In summary, we have successfully prepared $CsPbBr_3$ thin films by thermal co-evaporation. We studied the effects of co-evaporation rate ratio, substrate temperature, and annealing conditions on the properties of the films. We found that the optimal deposition conditions of $CsPbBr_3$ films were substrate temperature of 150 ℃ and evaporation rate ratio of $PbBr_2$ to CsBr of 3:1, and as-deposited films had high crystallinity and excellent stability. Furthermore, overall films showed the obvious luminescence peak near 517 nm, with narrow FWHM. In addition, by introducing the annealing process, we found that with increasing annealing temperature and time, the films tended to be flatter with larger grain sizes. The PL intensity of $CsPbBr_3$ films also had variation tendency, which were consistent with XRD and SEM analysis. The best annealing condition was at 460 ℃ for 60 s, which could achieve the strongest PL intensity and the best crystallinity with large grains up to 3 μm. Once exceeding this value, PL intensity and crystallinity of $CsPbBr_3$ films began to decline. The obtained films with large grain sizes and high quality have a very broad application prospect. These provide a basis for further large-scale production of stable, efficient, and all inorganic $CsPbBr_3$ optoelectronic devices. The corresponding LEDs had a very good color purity, which could work continuously for 12 h in ambient air, with relatively superior stability.

Acknowledgements

The authors thank Shenwei Wang for his suggestions on their manuscript.

Author contributions

TB wrote the main manuscript. SW, LB, KZ and CC read and approved the final manuscript. LY contributed to funding acquisition. All authors read and approved the final manuscript.

Funding

This study was supported in part by grants from the National Natural Science Foundation of China (Grant No. 61975008).

Availability of Data and Material

All data generated or analyzed during this study are included in this published article.

Declarations

Ethics Approval and Consent to Participate

Not applicable.

Consent of Publication
Not applicable.

Competing interests
The authors declare that they have no competing interests.

Received: 23 March 2022 Accepted: 26 July 2022
Published online: 02 August 2022

References

1. Conings B, Drijkoningen J, Gauquelin N (2015) Intrinsic thermal instability of methylammonium lead trihalide perovskite. Adv Energy Mater 5(15):1500477
2. Swarnkar A, Chulliyil R, Ravi VK (2015) Colloidal $CsPbBr_3$ perovskite nanocrystals: luminescence beyond traditional quantum dots. Angew Chem Int Ed 54(51):15424–15428
3. Dong Y, Qiao T, Kim D (2018) Precise control of quantum confinement in cesium lead halide perovskite quantum dots via thermodynamic equilibrium. Nano Lett 18(6):3716–3722
4. Liu B, Wang L, Gu H (2018) Highly efficient green light-emitting diodes from all-inorganic perovskite nanocrystals enabled by a new electron transport layer. Adv Opt Mater 6(11):1800220
5. Wang N, Cheng L, Ge R (2016) Perovskite light-emitting diodes based on solution-processed self-organized multiple quantum wells. Nat Photonics 10(11):699–704
6. Hoye RLZ, Chua MR, Musselman KP (2015) Enhanced performance in fluorene-free organometal halide perovskite light-emitting diodes using tunable, low electron affinity oxide electron injectors. Adv Mater 27(8):1414–1419
7. Tiwari A, Satpute NS, Mehare CM (2021) Challenges, recent advances and improvements for enhancing the efficiencies of ABX_3-based PeLEDs (perovskites light emitting diodes): a review. J Alloy Compd 850:156827
8. Liu B, Hu S, Zhang L (2021) Blue molecular emitter-free and doping-free white organic light-emitting diodes with high color rendering. IEEE Electron Device Lett 42(3):387–390
9. Xiao P, Huang J, Yan D (2018) Emergence of nanoplatelet light-emitting diodes. Materials 11(8):1376
10. Chen W, Zhang J, Xu G (2018) A semitransparent inorganic perovskite films for overcoming ultraviolet light instability of organic solar cells and achieving 14.03% efficiency. Adv Mater 30(21):1800855
11. Murugadoss G, Thangamuthu R (2019) Metals doped cesium based all inorganic perovskite solar cells: investigations on Structural, morphological and optical properties. Sol Energy 179:151–163
12. Jingru ZG (2019) All-inorganic $CsPbX_3$ perovksite solar cells: progress and prospects. Angewandte Chemie (International ed. in English)
13. Zhang Y, Luo L, Hua J (2019) Moisture assisted $CsPbBr_3$ films growth for high-efficiency, all-inorganic solar cells prepared by a multiple sequential vacuum deposition method. Mat Sci Semicon Proc 98:39–43
14. Hu Y, Wang Q, Shi Y (2017) Vacuum-evaporated all-inorganic cesium lead bromine perovskites for high-performance light-emitting diodes. J Mater Chem C 5:133
15. Shi Y, Wu W, Dong H (2018) A strategy for architecture design of crystalline perovskite light-emitting diodes with high performance. ADV Mater 30(25):1800251
16. Xiao Z, Kerner RA, Zhao L (2017) Efficient perovskite light-emitting diodes featuring nanometre-sized crystallites. Nat Photonics 11(2):108–115
17. Zhang F, Sun M, Luo X (2020) Modulation of ligands conjugation for efficient $FAPbBr_3$ based green light-emitting diodes. Mater Chem Front 4:3001
18. Lee SJ, Shin SS, Kim YC (2016) Fabrication of efficient formamidinium tin iodide perovskite solar cells through SnF_2-pyrazine complex. J Am Chem Soc 138(12):3974–3977
19. Wang J, Wang N, Jin Y (2015) Interfacial control toward efficient and low-voltage perovskite light-emitting diodes. Adv Mater 27(14):2311–2316
20. Wang Z, Cheng T, Wang F (2016) Morphology engineering for high-performance and multicolored perovskite light-emitting diodes with simple device structures. Small 12(32):4412–4420
21. Cao Y, Wang N, Tian H (2018) Perovskite light-emitting diodes based on spontaneously formed submicrometre-scale structures. Nature 562(7726):249–253
22. Wang H, Zhang X, Wu Q (2019) Trifluoroacetate induced small-grained $CsPbBr_3$ perovskite films result in efficient and stable light-emitting devices. Nat Commun 10(1):665
23. Lei J, Gao F, Wang H (2018) Efficient planar $CsPbBr_3$ perovskite solar cells by dual-source vacuum evaporation. Sol Energ Mat Sol C 187:1–8
24. Li J, Gao R, Gao F (2020) Fabrication of efficient $CsPbBr_3$ perovskite solar cells by single-source thermal evaporation. J Alloy Compd 818:152903
25. Ma Q, Huang S, Wen X (2016) Hole transport layer free inorganic $CsPbIBr_2$ perovskite solar cell by dual source thermal evaporation. Adv Energy Mater 6(7):1502202
26. Chen C, Lin H, Chiang K (2017) All-vacuum-deposited stoichiometrically balanced inorganic cesium lead halide perovskite solar cells with stabilized efficiency exceeding 11%. Adv Mater 29(12):1605290
27. Bai LY, Wang SW, Zhang YW (2020) Influence of annealing process on the stable luminous $CsPbCl_3$ perovskite films by thermal evaporation. J Lumin 227:117592
28. Shin M, Lee HS, Sim YC (2020) Modulation of growth kinetics of vacuum-deposited $CsPbBr_3$ films for efficient light-emitting diodes. ACS Appl Mater Interfaces 12(1):1944–1952
29. Tang ZK, Wong GKL, Yu P (1998) Room-temperature ultraviolet laser emission from self-assembled ZnO microcrystallite thin films. Appl Phys Lett 72(25):3270–3272
30. Cody GD, Brooks BG, Abeles B (1982) Optical absorption above the optical gap of amorphous silicon hydride. Solar Energy Materials 8(1):231–240
31. Zhou H, Zeng J, Song Z (2018) Self-powered all-inorganic perovskite microcrystal photodetectors with high detectivity. J Phys Chem Lett 9(8):2043–2048
32. Liu X, Tan X, Liu Z (2019) Sequentially vacuum evaporated high-quality $CsPbBr_3$ films for efficient carbon-based planar heterojunction perovskite solar cells. J Power Sources 443:227269
33. Duan J, Zhao Y, He B (2018) Simplified perovskite solar cell with 4.1% efficiency employing inorganic $CsPbBr_3$ as light absorber. Small 14:1704443
34. Lohmann KB, Patel JB, Rothmann MU (2020) Control over crystal size in vapor deposited metal-halide perovskite films. ACS Energy Lett 5(3):710–717
35. Oliveira J, Cavaleiro A (2006) Influence of substrate properties and annealing temperature on the stress state of magnetron sputtered tungsten thin films. J Vac Sci Technol 24:2070–2075
36. Thouless MD, Gupta J, Harper JME (1993) Stress development and relaxation in copper films during thermal cycling. J Mater Res 8:1845–1852
37. Keller RM, Baker SP, Arzt E (1999) Stress-temperature behavior of unpassivated thin copper films. Acta Mater 47:415–426
38. Kusaka K, Hanabusa T, Nishida M (1996) Residual stress and in-situ thermal stress measurement of aluminum films deposited on silicon wafer. Thin Solid Films 290–291:248–253
39. Zhou HM, Yi DQ, Yu ZM (2007) Preparation of aluminum doped zinc oxide films and the study of their microstructure, electrical and optical properties. Thin Solid Films 2:886
40. Shi D, Adinolfi V, Comin R (2015) Low trap-state density and long carrier diffusion in organolead trihalide perovskite single crystals. Science 347(6221):519–522
41. Wetzelaer GAH, Scheepers M, Sempere AM (2015) Trap-assisted non-radiative recombination in organic-inorganic perovskite solar cells. Adv Mater 27(11):1837–1841
42. Sun J, Lu J, Li B (2018) Inverted perovskite solar cells with high fill-factors featuring chemical bath deposited mesoporous NiO hole transporting layers. Nano Energy 49:163–171
43. Zhuang S, Ma X, Hu D (2018) Air-stable all inorganic green perovskite light emitting diodes based on $ZnO/CsPbBr_3/NiO$ heterojunction structure. Ceram Int 44(5):4685–4688
44. Liu B, Tao H, Su Y (2013) Color-stable, reduced efficiency roll-off hybrid white organic light emitting diodes with ultra high brightness. Chinese Phys B 22(7):450–453

Publisher's Note